UNIVERSITY OF
GLASGOW
Optoelectronics
Research Group

Report to EOARD

Title: Laser bars of intersubband mid-infrared semiconductor lasers

Date submitted: March 2000

Principal Investigator : C. N. Ironside

Name of Organisation :
Department of Electronics and Electrical Engineering,
University of Glasgow
Glasgow, G12 8LT.

Type of Organisation: University

Name of Contracting Organization: University of Glasgow

Name, Phone, Fax, Email of Person Authorized to Sign Contract:
Stuart McKissock
Senior Contracts Manager
Universtiy of Glasgow
Glasgow G12 8QQ
Tel: 0141 330 3255 Fax 0141 330 4035
Email:smckissock@mis.gla.ac.uk

Check to be made payable to: The Court of the University of Glasgow

Address and person to mail check to:
Stuart McKissock
Senior Contracts Manager
Universtiy of Glasgow
Glasgow G12 8QQ

Contact: C. N. Ironside (C.Ironside@elec.gla.ac.uk)

20000628 109

AQF00-09-2889

REPORT DOCUMENTATION PAGE

Form Approved OMB No. 0704-0188

1. AGENCY USE ONLY (Leave blank)	2. REPORT DATE March 2000	3. REPORT TYPE AND DATES COVERED Final Report

4. TITLE AND SUBTITLE

Laser Bars Of Intersubband Mid-IR Semiconductor Lasers

5. FUNDING NUMBERS

F61775-99-WE

6. AUTHOR(S)

Prof. Charles N. Ironside

7. PERFORMING ORGANIZATION NAME(S) AND ADDRESS(ES)

University of Glasgow
Glasgow G12 8LT
Scotland

8. PERFORMING ORGANIZATION REPORT NUMBER

N/A

9. SPONSORING/MONITORING AGENCY NAME(S) AND ADDRESS(ES)

EOARD
PSC 802 BOX 14
FPO 09499-0200

10. SPONSORING/MONITORING AGENCY REPORT NUMBER

SPC 99-4048

11. SUPPLEMENTARY NOTES

12a. DISTRIBUTION/AVAILABILITY STATEMENT

Approved for public release; distribution is unlimited.

12b. DISTRIBUTION CODE

A

13. ABSTRACT (Maximum 200 words)

This report results from a contract tasking University of Glasgow as follows: The contractor will investigate the operation of a monolithic array of quantum cascade lasers to obtain high power operation (>200mW average power) at high temperature (>77K) and deliver 10 quantum confined laser bar chips.

14. SUBJECT TERMS

EOARD, Quantum confined lasers, semiconductor lasers, Mid-IR lasers

15. NUMBER OF PAGES

38

16. PRICE CODE

N/A

17. SECURITY CLASSIFICATION OF REPORT	18. SECURITY CLASSIFICATION OF THIS PAGE	19. SECURITY CLASSIFICATION OF ABSTRACT	20. LIMITATION OF ABSTRACT
UNCLASSIFIED	UNCLASSIFIED	UNCLASSIFIED	UL

UNIVERSITY OF
GLASGOW
Optoelectronics
Research Group

1   Background

Semiconductor lasers sources operating in the mid infrared (mid-IR) the 3-20μm wavelength region, which were compact, robust, efficient, tunable, with powers in the 100mW region would significantly boost applications in sensing, infrared countermeasures and medical diagnostics.

Recent results from the Lucent group[1] on a laser emitting at a wavelength of 8 μm show, at room temperature, a record peak power of 325 mW and a record slope efficiency of 180 mW/A. In continuous-wave operation the maximum power at 30 K was 510 mW per facet and still 200 mW per facet at 80 K. The total electrical-to-optical power conversion efficiency has been measured as 7% (at 20K), a value very close to the best value ~8.5% obtained for a QC laser emitting at 5 μm. This is in addition to demonstrating DFB lasers[2] and superlattice lasers[3] both at room temperature. This has all been demonstrated using InAlAs/InGaAs ternary layers lattice matched to InP, the wavelength of operation can be altered over the range 3.5-17μm by selecting different layer thicknesses.

This report covers the work carried out at the University of Glasgow during the period Sept 1990-February 2000 on high powered Quantum Cascade Lasers (QCL). The work was mostly carried out by Mr. C. Farmer who was the research assistant on the project.

1.1   Objective of the research work:

The objective of the research was:-
(1) Investigate the operation of a monolithic array of quantum cascade lasers to obtain high power operation (>200mW average power) at high temperature (>77K).

[1]C.Gmachl et al. Appl. Phys. Letts 72 3130 1998.
[2]J.Faist et al "Distributed feedback quantum cascade lasers" Appl. Phys. Lett. 70 2670-2672 1997.
[3] A. Tredicucci et al. "High-Power interminiband lasing in intrinsic superlattices" Appl. Phys Letts. 72 2388 1998.

2   QC Laser Arrays

2.1   Why use a laser array?

To achieve high average optical output powers, a conventional QCL must be driven with high duty cycles. However, QCLs require both high currents and high voltages to operate, and only a small percentage (<10%) of the electrical power supplied is converted to light; most of the electrical power just produces heat in the active region which rapidly deteriorates the laser performance. Wide lasers produce high optical output powers, but it is broadly acknowledged that heat is dissipated faster in narrow devices. It may therefore be preferable to have a large number of narrow, spatially separated QCLs working in parallel on the same chip (i.e. a QCL array). This effectively spreads the heat generated over a much larger area, decreasing the effective thermal resistance. For a given optical output power, the active region temperature of each QCL in the array should be lower than it would for single device emitting the same optical power. The total heat generated (and therefore the heatsink temperature) should remain the same, but the heat should be more delocalised in the laser chip. A schematic drawing (Figure 1) illustrates this point below. Black areas represent low temperature, and white areas indicate hot regions.

2.2   Choice of waveguide width for array

The optimal waveguide width for conventional mesa-etched QCLs with a silica dielectric layer, emitting at $\lambda \sim 5\mu m$, is around 10-20μm. Waveguides lower than ~10μm exhibit higher threshold current densities arising from an increased interaction of the optical mode with the waveguide sidewalls and their coatings (silica and metal contact layers).   A waveguide width of ~10-14μm was therefore chosen for the QC array lasers.
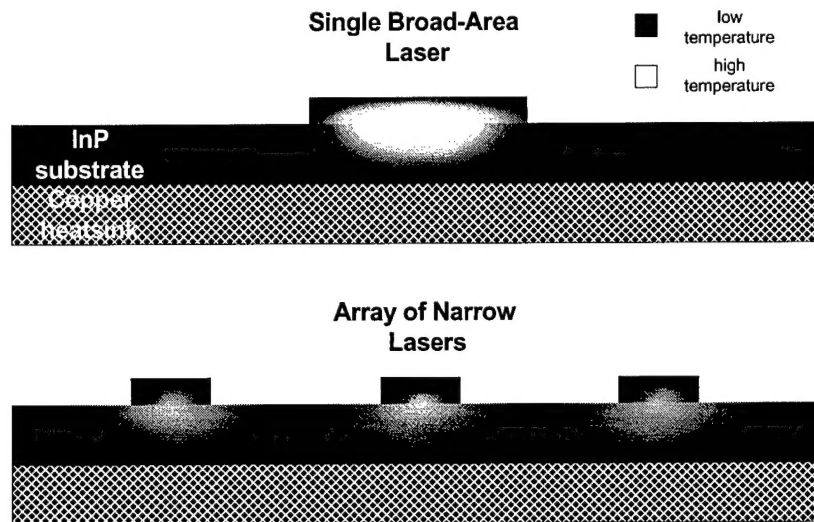
Figure 1

2.3   Choice of substrate thickness for array

The laser chip is usually mounted onto a copper heatsink which has very good thermal conductivity. The InP substrate conducts the heat away from the each laser to the copper heatsink. Unfortunately, the thermal resistance of the InP is relatively high ($K < 68$ W m^{-1} K^{-1} at T = 300 K) compared to that of the copper ($K \approx 400$ W m^{-1} K^{-1} at T = 300 K) and it therefore acts as a barrier to heat dissipation. In order minimise thermal resistance between each laser waveguide and the copper heatsink, and to facilitate cleaving, the InP substrate is thinned to ~150 μm. This is a practical minimum thickness.

UNIVERSITY OF
GLASGOW
Optoelectronics
Research Group

2.4 Choice of waveguide separation for array

As discussed previously, the thermal conductivity of the copper heatsink is far superior to that of the InP substrate. The InP in close proximity to the copper will be at a temperature close to that of the copper itself. However, the temperature of the InP adjacent the active region of each laser will be elevated by the heat generated there. This situation results in a thermal gradient across the InP between the copper heatsink and each device. If the distance between the active region and the copper heatsink is short (i.e. the InP substrate is thin), this thermal gradient will be very steep. Under these conditions the phonons (heat) will preferentially diffuse towards the heatsink, rather than laterally towards its neighbouring waveguides in the array.

It is safe to assume then that if the substrate is thinned to 150μm, then a separation of 150μm between the each waveguide should be sufficient to prevent heat localisation of heat.

A value of 150 μm was also considered to be practical when considering that if the array is to include a large number of devices, the total width of the array chip width must not be excessive.

3 Layer Sequence for QC Wafer A1376

Wafer A1376 was employed in for all the quantum cascade lasers reported here. Table 1 provides a description of the wafer which was grown by molecular beam epitaxy by the MBE group headed by Prof. Colin Stanley in the Dept. Of Electronic & Electrical Eng., University of Glasgow. The wafer design was based on a design first published by the Lucent group.[4]

Table 1 The Quantum Cascade Laser wafer (A1376)

Repeats	Material	Thickness	Unit	Doping	Impurity
1	InGaAs	200	A	2E19 cm-3	Si
1	InAlAs-InGaAs grade	300	A	7E18 cm-3	Si
1	InAlAs	12000	A	7E18 cm-3	Si
1	InAlAs	7000	A	3E17 cm-3	Si
1	InAlAs	6000	A	2E17 cm-3	Si
1	InGaAs-InAlAs grade	300	A	2E17 cm-3	Si
1	InGaAs	1500	A	1E17 cm-3	Si
25	InAlAs	23	A		
25	InGaAs	22	A		
25	InAlAs	22	A		
25	InGaAs	20	A	2E17 cm-3	Si
25	InAlAs	20	A	2E17 cm-3	Si
25	InGaAs	20	A	2E17 cm-3	Si
25	InAlAs	23	A		
25	InGaAs	19	A		
25	InAlAs	28	A		
25	InGaAs	19	A		
25	InAlAs	50	A		
25	InGaAs	10	A		
25	InAlAs	15	A		
25	InGaAs	47	A		
25	InAlAs	22	A		
25	InGaAs	40	A		
25	InAlAs	30	A		
25	InGaAs	23	A		
1	InAlAs	23	A		
1	InGaAs	22	A		
1	InAlAs	22	A	2E17 cm-3	Si
1	InGaAs	20	A	2E17 cm-3	Si
1	InAlAs	20	A	2E17 cm-3	Si
1	InGaAs	3000	A	1E17 cm-3	Si
1	InAlAs-InGaAs grade	300	A	1E18 cm-3	Si
1	InAlAs	50	A	1E18 cm-3	Si
1	InP	20000	A	1E18 cm-3	Si
Substrate	InP	–	A	1E18 cm-3	?

[4] J. Faist, F. Capasso, C. Sirtori, D.L. Sivco, J.N. Baillargeon, A.L. Hutchinson, S.G. Chu, A.Y.Cho, 'High power mid-infrared (λ~5 µm) quantum cascade lasers operating above room temperature', *Appl. Phys. Lett.* **68** (26), 24 June 1996.s

3.1   Results from Single Stripe QC Lasers fabricated from Wafer A1376

Conventional QC lasers were fabricated from wafer A1376 to establish a starting point for the fabrication of array laser. These laser were fabricated using an identical fabrication process as for the array laser (detailed in sections ahead), except that the device separation was 500μm to allow cleaving into single laser bars of 2mm and 3mm length. The devices were mounted epi-layer up on T0-5 heatsinks with indium and wire-bonded using an ultrasonic wire-bonder.

The lasers were placed on the cold finger of a closed-cycle continuous-flow helium cryostat with optical access. Light from the lasers was collected using gold-coated parabolic mirrors and focused onto a calibrated liquid nitrogen-cooled mercury cadmium telluride (MCT) detector. The lasers were driven with 100ns current pulses with a repetition rate of 5kHz. The spectra were taken using a Fourier transform infrared (FTIR) spectrometer operating in step-scan mode.
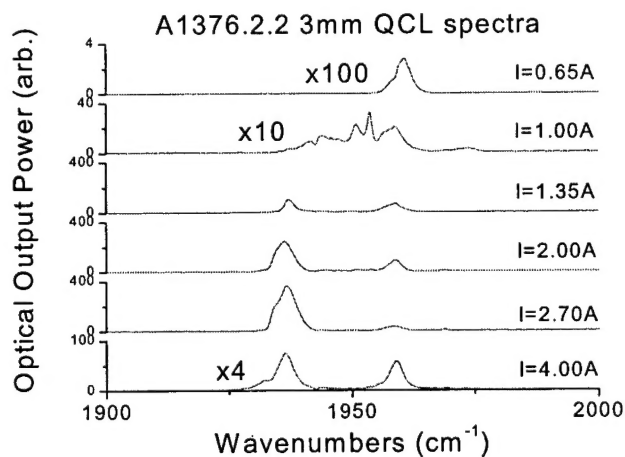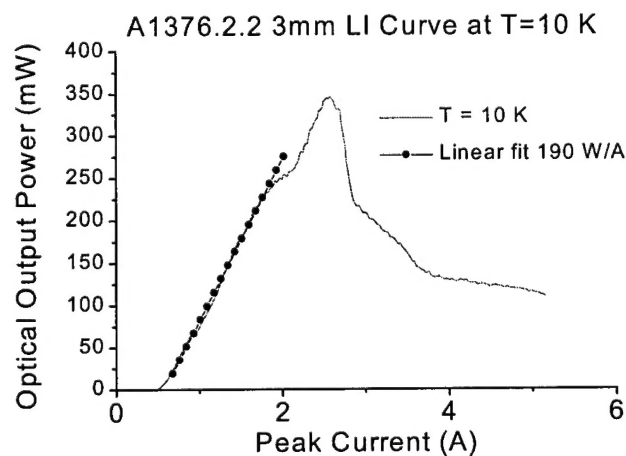
Figure 2 QCL Spectra

Figure 3 Light-Current curves for various temperatures for a 3 mm-long laser.

A1376.2.3 2mm QCL LI curve
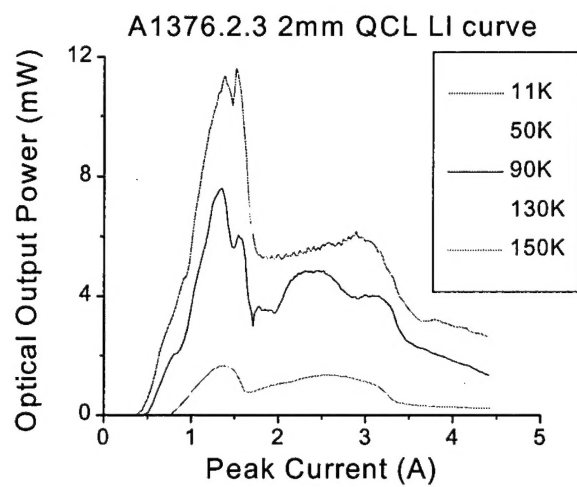
Figure 4 Light-Current curves for various temperatures for a 2 mm-long laser.

4 Fabrication of the QCL laser chip

4.1 QCL Array photolithographical mask pattern

Below is a schematic representation (to scale) of the photolithographical mask used for the QCL array laser fabrication. The top part of the Figure 5 represents a zoomed view of a small section of the complete mask (bottom part of figure). The black regions represent ferric areas which blocks the UV light, and the grey areas are transparent to the UV light. The ferric lines which will define the width of each individual QC laser waveguide are 16 μm wide, and the transparent areas, which define the inter-waveguide separation, are 150 μm wide. The length of the each line is 6 mm.

Figure 5 Schematic of the photolith mask

4.2   Fabrication Process

contact window on ridge waveguide

InP substrate

reverse contact

Figure 6 Fabrication of a single stripe.

4.2.1   Formation of the ridge waveguides
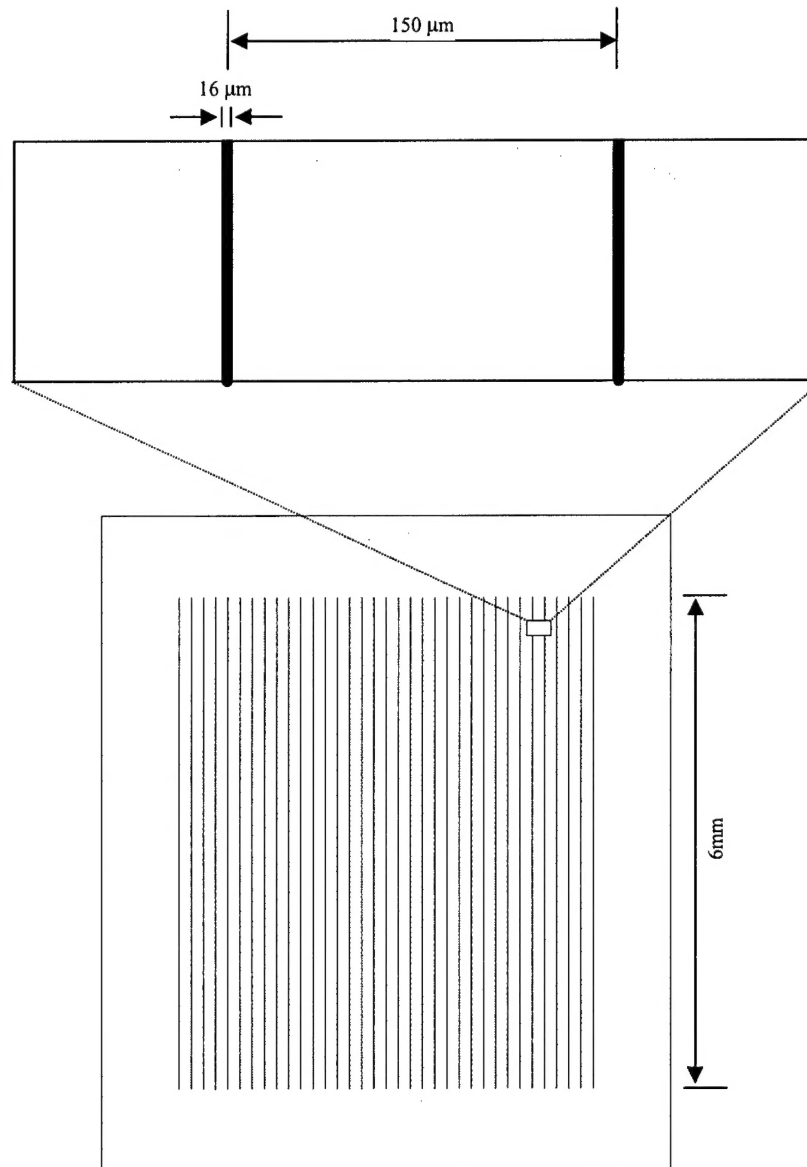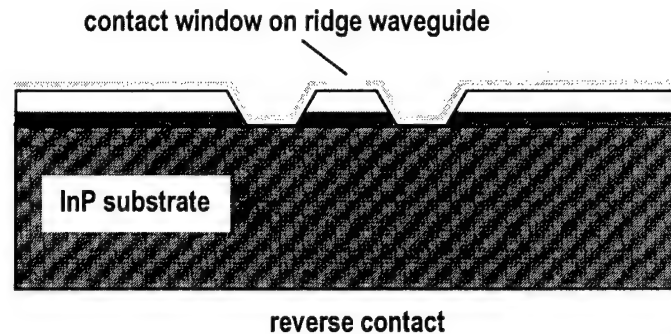
The following steps lead to the formation of the optical ridge waveguides. Parameters such as the ridge height and width, and spacing are defined by these steps. The ridge height is determined by the vertical etch rate, etch time and selectivity to different layers. The ridge waveguide width and spacing are determined by the mask, and the horizontal etch rate (undercut) and profile.

The waveguide pattern must be parallel to the edge of the sample to permit the formation of mirrors normal to the laser cavity through cleaving. In the case where a crystallographic etch is used, this edge must be the appropriate crystal plane in order to produce the desired sidewall profile. Details of the etch and mask pattern used are given in previous sections.

1. Scribe and cleave wafer into rectangular areas 8 mm parallel to the major flat $[0\overline{1}\,\overline{1}]$ and 7 mm parallel to the minor flat $[0\overline{1}1]$. *To give clear indication of crystal plane direction if a crystallographic etch is to be used.*
2. Cleaning procedure: 5 mins ultrasonic in Opticlear, rinse with acetone. 5 mins ultrasonic in acetone, rinse with methanol. 5 mins ultrasonic in methanol, rinse well with running RO water. Blow dry.
3. Spin resist procedure: spin S1818 resist for 30s at 4000 rpm. Carefully remove large resist build-up from corners with flat end of tweezers.
4. Pre-bake resist procedure: place on a petri dish in an oven at 90°C for 30 mins.
5. Expose resist on outer periphery of sample. Requires large exposure time, approx. 50 secs due to greater resist layer thickness. *Will allow close contact of next mask and prevent breakage of sample arising from an uneven distribution of mask-sample contact.*
6. Remove mask from the mask aligner and turn sample face down. Expose reverse surface for approx. 70 secs. *Will facilitate good parallelism of the sample to the etch mask by removal of unwanted resist on the underside of the sample.*
7. Develop resist procedure: thoroughly mix 1:1 solution of S1818 developer and RO water. Place sample in a petri dish containing the mixed solution for 75 secs, agitating the sample every 15 secs. Rinse well in RO water. Blow dry.
8. Place in oven at 90°C for 3 mins. *Evaporate any residual water from surface.*
9. Align the array mask pattern (see sectioned titled 'QCL Array photolithographical mask pattern' for details of the pattern used) such as to give ridges parallel to long edge of sample (major flat). Bring mask into contact and expose for normal S1818 time (10 seconds).
10. Repeat developing procedure (step 7).
11. Post-bake resist procedure: place on a petri dish in an oven at 120°C for 30 mins. Let sample cool.
12. Prepare the etch - see etch information for preparation details.

UNIVERSITY OF
GLASGOW
Optoelectronics
Research Group

Table 2 Etch recipe

Etch name	Orthophosphoric
Substrate	InGaAs/AlInAs/InP
Chemicals	$H_3PO_4:H_2O_2:H_2O$
Ratio	1:1:8
Temperature	room temperature
Etch rate	1.4 μm/min vertically, 1 μm/min horizontally
Selectivity	stops on InP
Sidewall angle	55 ° parallel to the [0 $\bar{1}$ $\bar{1}$] crystal plane, 115 ° parallel to [0 $\bar{1}$ 1]
Comments	do not stir
Source	A. Stano, 'Chemical Etching Characteristics of InGaAs/InP and InAlAs/InP Heterostructures', J. Electrochem. Soc., 134 (2) 448, February 1987.

13. Etch exposed epilayers: see individual etch information for etch conditions and rates.
14. Once etching is completed, remove the resist etch mask using an ultrasonic bath in acetone for 2 mins followed by rinses in methanol and RO water. Blow dry.

4.2.2 Insulation layer

Since the waveguides are very narrow, it is not possible to wire bond an electrical connection to them directly and therefore a broad contact area is incorporated into the design. The electrical contact must only be made to the very top of the ridge and so a dielectric layer is needed to provide electrical insulation between the remaining semiconductor surface and the metal contact layer.

1. Deposit 400 nm of PECVD silica. *The metal contact layer sticks well to sputtered silica.*
2. Spin resist procedure.
3. Pre-bake resist procedure.
4. Expose outer periphery with 'exposedge2' mask pattern for approx. 70 secs. *The new periphery exposure mask is needed to include the removal of the build-up at the step etched as a consequence of the 'exposedge' mask used in step 5 of the ridge formation.*
5. Remove mask from the mask aligner and turn sample face down on a piece of rubylith. Expose reverse surface for approx. 50 secs.
6. Develop resist procedure.
7. Place in oven at 90°C for 3 mins.
8. Align appropriately sized windows to ridge plateau centres. 4μm windows were used for our array lasers. *This requires a mask with window widths approximately equal to plateau width minus 4-6μm.* Bring the mask into contact and expose for 60% normal exposure S1818 time using Karl Suss mask aligner. *Exposure time is reduced since the S1818 resist was found to be less than 60% of its normal thickness on the ridge (only 1μm rather than 1.8 μm).*
9. Develop resist procedure.
10. Post-bake at 90°C for 30 mins. *Higher temperatures will cause resist to flow into etched trenches, leaving sidewalls exposed.*
11. Dry etch silica in C_2F_6 for 5 mins. *Wet etching exposes the ridge sidewalls by undercutting the resist. Dry etching is necessary.*

4.2.3 Contacts

The aims of the next list of processing steps are to obtain ohmic contacts to the top of each ridge waveguide, and a broad, flat region which to wire bond to. The contacts are made to the top of ridge waveguide through the window in the silica. The wire bonding area will be provided in the strip adjacent to each ridge. The contact in that area is insulated from the substrate dielectric layer deposited earlier in the process.

1. Spin S1818 resist on a glass coverslip for few seconds. Place sample pattern-side-up onto slip and dry in oven for 30 mins. *Mounting of sample for contact deposition.*
2. Deoxidised in 1:1 HCl:H2O for 30 secs. Rinse in RO water. Dry in nitrogen oven for 30 mins at 90°C. *Prepares both InGaAs surface and silica surface for contact deposition*

3. Deposit a p-type contact (Ti/Pd/Au). *A p-type contact may be used as the InGaAs contact layer is very heavily n-type doped. The Ti/Pd/Au is preferential since it adheres well to the silica layer, allowing ultrasonic wire bonding.*

4. Rinse in acetone, methanol, then RO water and blow dry. Do not use ultrasonic cleaning!!

5. Spin S1818 resist on a glass coverslip for few seconds. Place sample pattern-side-down onto slip and dry in oven for 30 mins. *Mounting of sample for thinning and n-type contact deposition.*

6. Mount coverslip onto metal chuck with wax. *Use of coverslip avoids contact of wax with sample.*

7. Thin InP substrate from 400 μm to ~200μm with 9μm aluminium oxide powder and from 200 μm to 160 μm with 3μm aluminium oxide powder. Heat chuck until wax just melts and remove the coverslip. Polish sample by etching from 160 μm to 150 μm with HBr:Nitric:H2O. *Thinning reduces the distance from the epilayer to the heatsink and improves the cleaving process.*

8. Repeat steps 14 to 15, but deposit an n-type contact (Au/Ge/Au/Ni/Au). *Reverse contact deposition on the InP substrate.*

9. Remove from coverslip with acetone, rinse with methanol, RO water, then blow dry.

4.3 Cleaving process

The sample is now ready to be cleaved up into sets of lasers. In this stage the laser cavity mirrors are formed and the length of the laser cavity is defined.

4.4 Mounting on to a copper block

The QCL chip was mounted on a copper block which acted as a heat sink. The mount was designed to fit into a cryostat (see below for description of cryostat). The QCL chip was bonded on to the copper block with indium solder which provided a good thermal and electrical contact.

5   Results and characterisation of the QC laser array

The QC laser array was characterised by several sets of measurements which included:

- measuring the current-voltage (I-V) of the laser chip,
- measuring the light - current (L-I) curves at a series of temperatures to determine the threshold current as a function of temperature,
- measuring the spectrum of the light emitted from the laser,
- and mesauring the spatial distribution of the light intensity in directions perpendicular to the direction of propagation - the so-called mode profile.

To undertake these measurements the laser chip was mounted on a copper block which served as a heat sink. The mount was coated with indium and the laser chip soldered on. The copper block was with the bonded laser chip was then mounted on the end of a sample rod that fitted into an Oxford Instrument CCC1204 top-loading closed-cycle continuous flow cryostat. The cryostat was capable of operating in the temperature range 11 K to 320 K with a typical cooling power of 1.5 Watts. The windows of the cryostat were IR transparent (Zinc Selenide).

The laser chip power pulsed supply comprised:

Del Power RHVS-500
DEI HV1000 negative polarity unit 220VAC
B-1010 TTL pulse generator

The system was capable of supplying current pulse of amplitudes between 0 and 17A, and pulse widths above 100ns with duty cycles up to 10% (at 2A). A multi-channel Stanford Instruments boxcar averager with a digitising computer interface module was used to collect and perform noise reduction on the data before sending it to a computer for data logging.

The results reported here are for 3x1 QCL laser arrays, that is three laser stripes of width 14μm separated by 150μm and 2.6mm long on the same chip. Typically the laser chip was run with pulse widths around 200ns. In order to impedance match to the transmission line which delivered the pulses from the power supply to the laser chip, it was necessary to have an impedance matching circuit before the input to the cryostat. The impedance matching circuit consisted of a non-inductive, high-power thin metal film (wire wound resistors must NOT be used!) 50 Ω resistor in series with the laser chip. The magnitude of the current pulse was measured using a 711S current probe.

5.1   The I-V characteristic of the QCL array
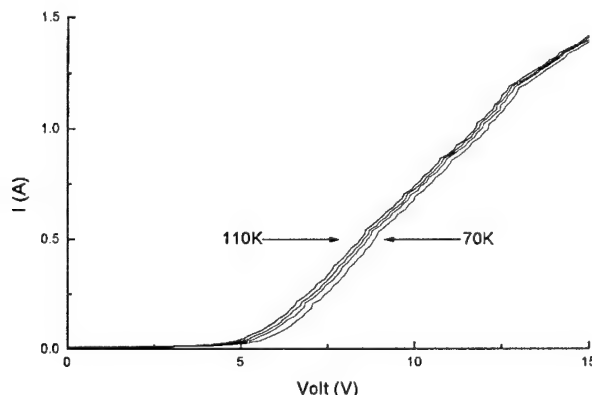

Figure 7 The I-V of the QCL laser array chip

The I-V characteristic of the laser chip shows that typically to obtain current turn-on a voltage of 5V has to be applied. The I-V characteristics of quantum cascade laser are markedly different from

conventional interband lasers that employ a pn junction. From the I-V curve shown in Figure 7, the laser chip does not start to conduct until sufficient voltage has been applied to produce an electric field that aligns the energy the various levels and minbands in the active region. The electrons can then be transported through the layers.

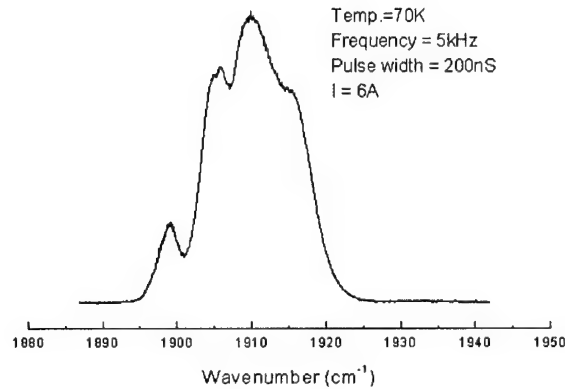## 5.2   The spectrum of the QCL array

Figure 8 The figure shows the measured distribution of light intensity versus wavelength for an QCL array. The operating conditions are shown on the diagram.   The peak wavelength is around 5230nm.

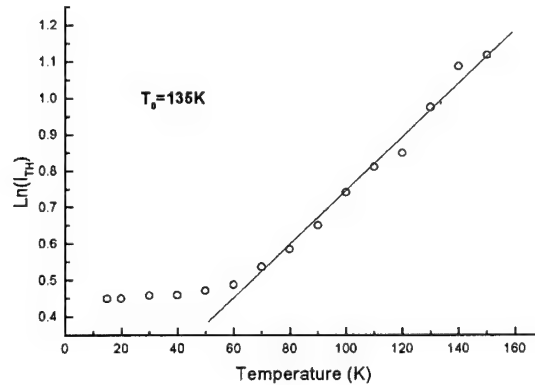## 5.3   Threshold current versus temperature

Figure 9 The temperature dependence of threshold current for the QCL laser array chip. The figure shows the natural log of threshold current versus temperature of the heat sink for the QCL array, the measurements were taken using the cryostat and current pulse of 200ns and 5kHz repetition frequency at a duty cycle of 0.1%. The gradient of straight line fit for temperatures over 60K gives the T_0 of the laser array.

The measured T_0 of 135K compares with 110K for a single stripe laser; this indicates that adding extra stripes at this spacing of 150μm does not incur a decrease in T_0 ; there is no penalty of an increased temperature dependence of the threshold current.

5.4 Mode Profiles
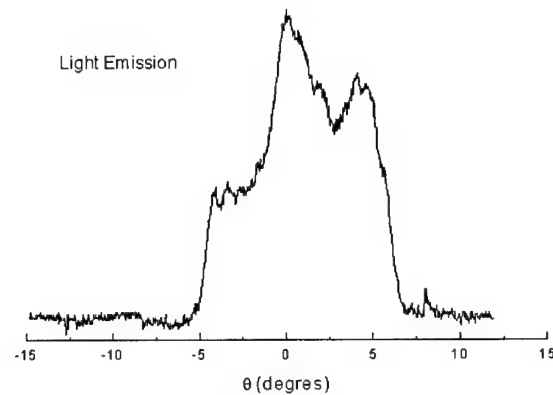
Light Emission

θ (degres)

Figure 10 The mode profile of the QCL laser array chip. The figure shows the distribution of light intensity in a direction perpendicular to the propagation direction of the light, parallel to the lateral direction of the chip. This is a far-field measurement at 42mm from the laser chip.

Figure 10 shows three peaks which is expected from a three stripe array. In the other direction, the vertical direction, the mode profile was single-lobed with a diffraction angle approximately 5 times larger than the lateral direction shown here.

5.5 Light current curves

Temp.=70K
Frequency = 5kHz
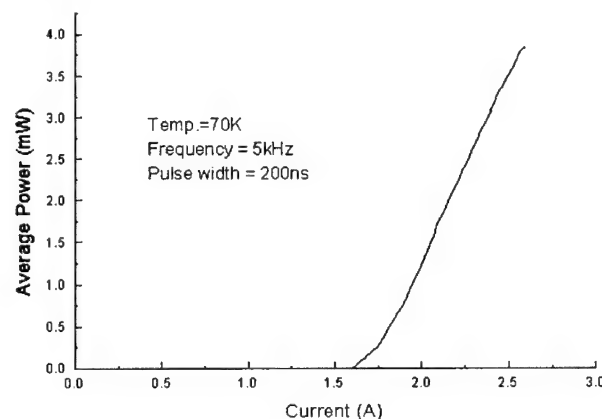Pulse width = 200ns

Average Power (mW)

Current (A)

Figure 11 The L-I curve of the QCL laser array chip. The figure shows the output light power per facet versus input current for QCL laser array; the operating conditions are shown; the duty cycle was 0.1%.

The light current curve was calibrated using the manufacture's data for the conversion efficiency of the detector and account was taken of the collection efficiency of the detector. The detector was a mercury cadmium telluride (MCT) detector of area 1mm x 1mm. The collection efficiency of around 0.7% is estimated from the beam profile measurements. Because the beam profiles are not simple Gaussians, the error margin of this calibration may be as large as 50%. At this duty cycle, the peak power for 1mW average power is 1W.

From the I-V curve and L-I curves, for 1mW average optical output power (1W peak power), the average power supplied to the laser was 0.05W (50W peak power), the efficiency is around 2% (wall plug). On average the heat sink is dissipating ~0.05W.

6   Non-linear Finite Element Analysis for Thermal Modelling of QCLs

Above we put forward arguments supporting the use of laser arrays for reducing the temperature of the active region of each laser. In this section, we report on computer modelling which was used to investigate the validity of the arguments.

6.1   Mathematical Description of Problem

Non-linear finite element analysis was used to solve the thermal diffusion equation,

$$\frac{\partial}{\partial x}\left(K_x\frac{\partial T}{\partial x}\right) + \frac{\partial}{\partial y}\left(K_y\frac{\partial T}{\partial y}\right) + \frac{\partial}{\partial z}\left(K_z\frac{\partial T}{\partial z}\right) + S = \rho C_p \frac{\partial T}{\partial t},$$

where, T is the temperature in Kelvin (or °C, if desired), K_x , K_y, and K_z (units in W m^{-1} K^{-1}) are the thermal conductivities in the x, y and z directions respectively, S is the value of the heat source (W m^{-3}) in any heated regions; the active regions of the QCL in this case, elsewhere it is zero. C_p (J kg^{-1} K^{-1}) and ρ (kg m^{-3}) are the specific heat and density of the material, the product of which gives the heat capacity (J m^{-3} K^{-1}).
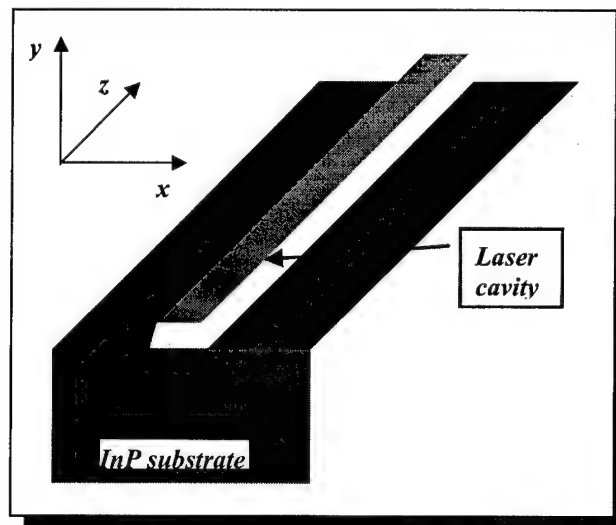

Figure 12 Simplified schematic drawing of the semiconductor laser diode and chosen coordinate system.

Referring to Figure 12, the x-axis was designated as the direction parallel to the semiconductor layers (or the 'lateral' direction). The y-axis was designated as the direction perpendicular to the semiconductor layers, but perpendicular to the longitudinal cavity of the laser. The z-axis lay parallel to the longitudinal laser cavity i.e. orthogonal to the x and y axes.

Assuming there is no net flow of heat along the laser cavity (in the z-direction), $\delta T/\delta z = 0$. The problem then becomes a two-dimensional one and the equation simplifies to,

$$\frac{\partial}{\partial x}\left(K_x\frac{\partial T}{\partial x}\right) + \frac{\partial}{\partial y}\left(K_y\frac{\partial T}{\partial y}\right) = \rho C_p \frac{\partial T}{\partial t}.$$

This can be solved using a finite element analysis program for solving partial differential equations. Further simplifications were made by assuming that the thermal conductivities of the materials involved were isotropic, i.e. $K_x = K_y = K$. Also, it was possible to solve the time-dependant equation

16

which would have allowed us to calculate the evolution of the temperature over time, but we are mainly interested in the equilibrium temperature reached, so the time-dependant version was not used. For steady state conditions, $\delta T/\delta t = 0$, so the right-hand-side may be set to zero and the equation then becomes,

$$\frac{\partial}{\partial x}\left(K\frac{\partial T}{\partial x}\right) + \frac{\partial}{\partial y}\left(K\frac{\partial T}{\partial y}\right) + S = 0.$$

The thermal conductivity of semiconductor (or metal) is temperature-dependant. The value of K at any given point (x, y) will be determined by the material and the temperature of the material at that point. This makes the problem non-linear, since calculating the temperature distribution requires a previous knowledge of the thermal conductivity distribution, which is itself temperature-dependant. The finite element analysis package employs an iterative process to solve the non-linear, partial differential equation,

$$\frac{\partial}{\partial x}\left(K(T)\frac{\partial T}{\partial x}\right) + \frac{\partial}{\partial y}\left(K(T)\frac{\partial T}{\partial y}\right) + S = 0.$$

In the calculations performed the following assumptions and approximations were made:

1. The temperature-dependence of the values of thermal conductivity of InP, InGaAs, InAlAs, and He gas were approximated using polynomials given in Table 3. The ternary semiconductor compounds InAlAs and InGaAs were described of polynomial equation.

Material	Thermal Conductivity (W m^{-1} K^{-1})
InP	$406 - 2 * T + 2.88\,E^{-3} * T^2$ [5]
InAlAs	$29 - (1.39E^{-1} * T) + (1.98\,E^{-4} * T^2)$ [5]
InGaAs	$29 - (1.39E^{-1} * T) + (1.98\,E^{-4} * T^2)$ [5]
Alumina (Al$_2$O$_3$)	3
Copper	398
Indium	81.8
Helium gas	$1.63E^{-2} + (6.12E^{-4} * T) - (5.49E^{-7} * T^2)$ [6]

Table 3. Thermal conductivity values used in the calculations.

2. The active region comprises of nearly 500 very thin (ranging between 0.9 to 5 nanometers in thickness) epitaxial layers; a superlattice of alternating InAlAs and InGaAs layers. These were much too thin to be modelled as individual layers (layers with dimensions no less than 500 nm were permitted in this model), and so were grouped together and approximated as a single layer.
3. The active region was assigned a thermal conductivity of bulk ternary material. This simplification ignores the reflection of phonons (heat) at each InAlAs/InGaAs interface in the superlattice. In practice this phenomenon would make the effective thermal conductivity of the superlattice anisotropic. The value of K_y, the thermal conductivity perpendicular to the semiconductor layers, would be reduced with respect to K_x.
4. The values of thermal conductivities used for indium and copper were those reported for pure materials at room-temperature and were assumed to be constant with temperature.
5. The values of thermal conductivities used were those reported for un-doped layers; values for doped semiconductors may be significantly lower. The modelling was performed on what was effectively an undoped semiconductor laser, whereas doping levels in a quantum cascade laser can be high and vary throughout the epilayer (see Table 4). Addition of doping atoms to the crystal lattice may create crystalline imperfections upon which phonons will scatter, decreasing the thermal conductivity. Towards room-temperature, the dependence of the thermal conductivity on doping level may be weak, since at high temperatures phonon-phonon scattering should dominante. At low temperature, where phonon-phonon scattering is weak, the phonon-impurity scattering will dominate, and the value of K will with drop with increasing doping levels. The

---

[5] Gmachl *et al.* , *IEEE Photonics Technology Letters* **11**, 1369 (1999).
[6] Therm Database program.

values of temperature calculated by the modelling, should therefore be more accurate towards room-temperature. The temperatures calculated should always be an underestimate of the actual temperature since the thermal conductivity is over estimated at low temperatures.

Material	Layer Thickness (nm)	Doping Level (*E16 cm^{-3})
Ternary (InAlAs)	1200	700
Ternary (InAlAs)	700	30
Ternary (InAlAs)	600	20
Ternary (InGaAs)	300	10
Active region (InGaAs\InAlAs)	1143	2.6 (average)
Ternary (InGaAs)	300	10
Binary (InP)	15000	100

Table 4 Summary of major semiconductor layers of the QCL in reverse order of growth.

6. There is no net heat flow along the laser cavity (z-direction).
7. Cooling due to convection was neglected.
8. Cooling due to radiation of heat was neglected. This is a reasonable assumption as long as the temperature difference, ΔT, between the heated surface and its surroundings is not too high. The value of cooling via radiation can be expressed by, $c_{rad} = \sigma.(\Delta T)^3$, where c_{rad} is the cooling by radiation (W m^{-2} K^{-1}), $\sigma = 5.67$E-8 W m^{-2} K^{-4} is the Stefan-Boltzmann constant. For $c_{rad} = 1$ W m^{-2} K^{-1}, $\Delta T = 260$ K. Temperature differentials obtained in these calculations are lower than 150K, so that cooling by radiation of heat can be neglected.

In any case, for the purpose of supporting the arguments raised previously, we are not overly concerned with the absolute values produced by the modelling, but more in the general trends calculated for different geometric configurations.

6.2 *Geometric Description of Problem*

Reference should be made to the QC laser fabrication section for an understanding of the general QCL construction and geometry. For simplicity, the insulation and contact layers have been not been included in the modelling. These layers are very thin ~300nm, and as such could not be entered into the program. The program cannot resolve layers whose x or y dimension is $1/2000^{th}$ of the entire dimension of the problem. The model attempts to describe a QC laser mounted with indium onto a copper heatsink and placed in a cryostat at $T = 77$ K. The sequence of layers (in order for epilayer-up mounting) included in the model are as follows: helium, upper cladding layer, active region, lower cladding layer, InP substrate, indium, and copper. Regions of helium or alumina (Al_2O_3) were used to replace areas of the upper cladding, active region and lower cladding layers to emulate etched moats for 'Mesa-etched QCLs' or alumina moats for 'PSWOX QCLs' (see Appendix 1 for a description of the PSWOX QCL).

The program required that boundary conditions be set at the outer boundaries of the modelled geometrical space. To best reconstruct conditions in a cryostat, the boundaries were placed relatively far away from the laser chip and the temperature of the entire boundary was set to $T = 77$ K i.e. the bottom and sides of the copper block and the outer edges of helium gas were set to $T = 77$ K. The maximum distance of these boundaries from the chip was limited by the finite element analysis program used. The maximum dimensions of the entire geometric space could not exceed ~2000 times the minimum feature size in the geometric description.

The problem was described geometrically using the following parameters (please refer to Figure 13, Figure 14, and Figure 15 for where many of the parameters are described diagrammatically):

Parameter in diagrams	Parameter in code	Value\Description
W_{wg} (μm)	MesaTopWidth (m)	Variable
W_{moat} (μm)	MoatBaseWidth (m)	Variable
W_{moat} (μm)	MoatBaseWidth (m)	Variable
-	MoatDepth (m)	Constant = 4363 nm for single mesa and array mesa
		Constant = 2500 nm PSWOX mesa
-	LowerCladdingThickness	Constant = 330 nm
-	ActiveThickness	Constant = 1143 nm
-	UpperCladdingThickness	Constant = 2890 nm
φ	MesaSidewallAngleDeg	Constant = 55 degrees
T_{air}	AirThickness	1 mm
T_{Cu}	CuThickness	1 mm
T_{Cu}	HeatSinkWidth	2 mm
-	InThickness	5 μm
T_{Sub}	SubstrateThickness	150 μm
W_{Sub}	SubstrateWidth	500 μm

The following parameters were applied solely to the modelling of the array QC lasers:

Parameter in diagrams	Parameter in code	Value\Description	
D_{array} (μm)	MesaSpacing	Variable	(distance between mesa in the array)
-	NoMesaInArray	Constant = 3	(number of mesa in the array)

It should be noted that the value of waveguide width W_{wg} in the model actually corresponds to an average active region width of $W_{wg} + 2(3.46/\tan \phi)$ owing to the sidewall angle φ being less than 90°. A 'waveguide width' W_{wg} =5μm in the model therefore corresponds to an active region width of $5 + 4.85 \approx 10$μm. Values of $W_{wg} = 10$ μm and 15 μm correspond to an active region width of ~15μm and ~20 μm respectively. The reason for selecting the top of the mesa as the point of measurement was to

prevent the selection of a mesa width which has a plateau width = 0 i.e. the two sloping sidewalls meet at the top, leaving no contact layer on top of the mesa.
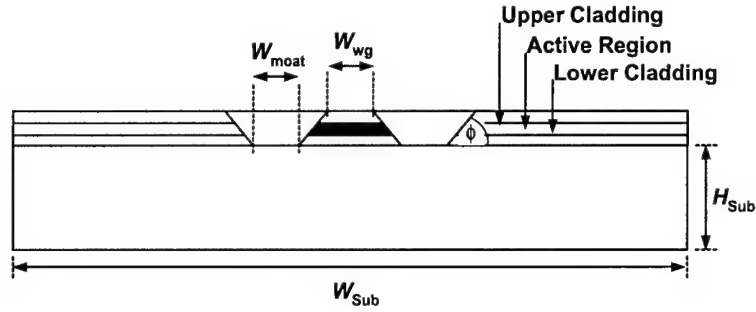
Figure 13 Geometric representation of the QCL used by the finite element analysis, showing the mesa sidewall angle ϕ, the width of the waveguide plateau W_{wg}, the width of the moat base W_{moat}, the thickness of the substrate H_{Sub}, the width of the substrate W_{Sub}, and the position of the upper cladding, active region and lower cladding layers. The area of the active region in solid black represents where the heat is generated.
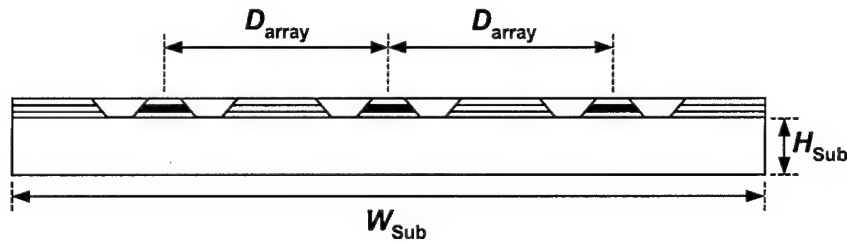

Figure 14 Geometric representation of the QC array laser used by the finite element analysis, showing the thickness of the substrate H_{Sub}, the width of the substrate W_{Sub}, and the distance D_{array} between individual mesa in the array. The areas of the active region in solid black represent where the heat is generated.
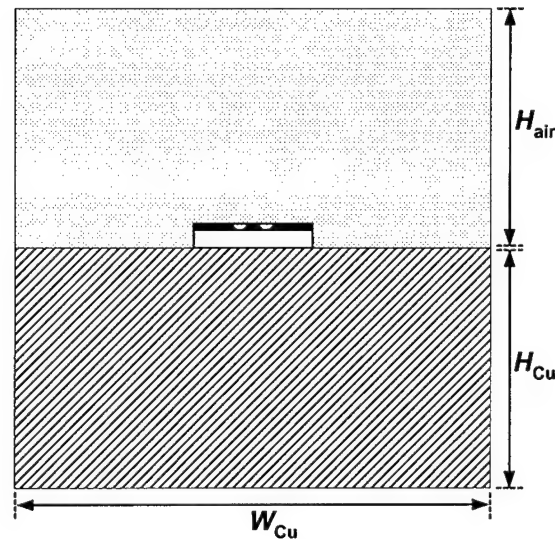

Figure 15 Geometric representation of the QC laser chip mounted epilayer-up onto a copper heatsink of width W_{Cu} and thickness H_{Cu}. The area, W_{Cu} by H_{air}, above the copper mount and laser chip is filled with 'air' (helium in our case).

6.3   Simulation results for Single Mesa QC Lasers

Firstly, effect of reducing the waveguide width while maintaining a constant input power density into the active region was modelled by using the combinations of W_{wg} and power given in Table 5. Results from the simulations are given in graph form in Figure 16 and in Figure 17, and the peak temperatures exhibited in each case are listed in Table 5. In both Figure 16 and Figure 18,   Position = 0 μm represents the InP substrate/epilayer interface. Position < 0 lies within the 'InP substrate', 0 < Position < 4.36μm contains the 'epilayer', and Position > 4.36μm represents 'air'. The 'Active Region' of the QCL lies 0.33μm < Position < 1.47μm.

This simulated reducing the laser width so as to produce a low threshold current (good) laser. However, this comes at the expense of a low output power (undesirable) device. The data confirms that, as one would expect, the laser temperature decreases as the laser width and input power are divided by the same factor.

W_{wg} (μm)	Power (W)	Peak temperature (K)
15	20	167
10	13.33	140
5	6.66	112

Table 5 Combinations of W_{wg} and power and the resultant value of peak temperature calculated.
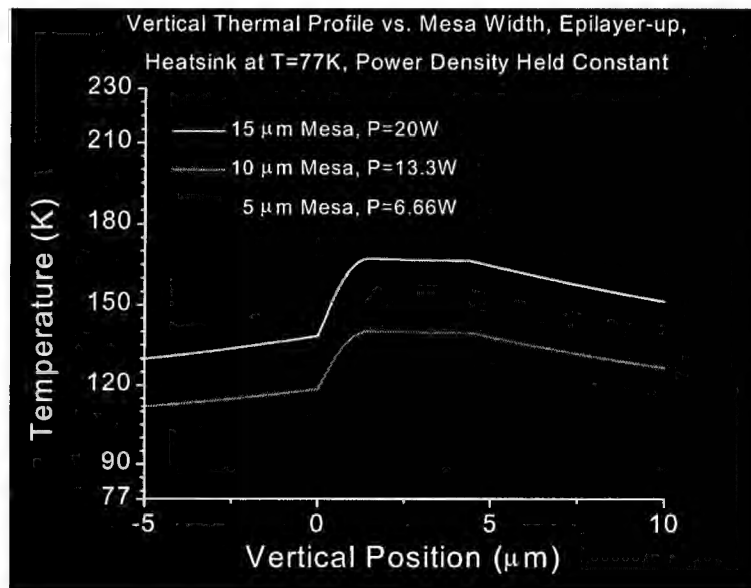

Figure 16 Calculation of the temperature profile through a vertical cross-section (down through the centre of mesa) of the QCL with the heatsink temperature set to T = 77 K. The calculation is shown for different values of mesa width (in the lateral direction), keeping the input thermal power density in the 'Active Region' constant in each case.
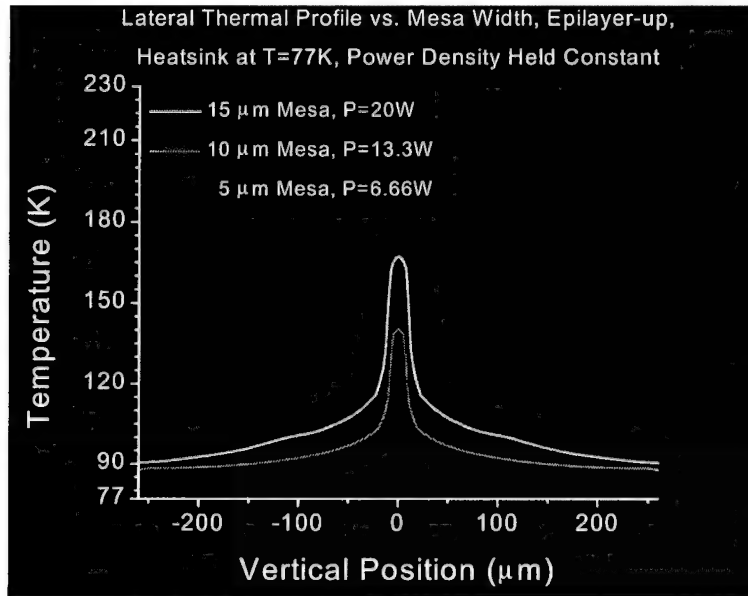
Figure 17 Calculation of the temperature profile through a lateral cross-section (along active region/upper cladding interface) of the QCL with the heatsink temperature set to T = 77 K. Position = 0 μm represents the centre of the mesa. The calculation is shown for different values of mesa width (in the lateral direction), keeping the input thermal power density in the 'Active Region' constant in each case.

Next, the effect of reducing the waveguide width while maintaining a constant generation of heat in the active region was modelled using a power of $P = 20$ W, and waveguide widths W_{wg} of 5, 10, and 15 μm. Results from the simulations are given in graph form in Figure 18 and in Figure 19, and the peak temperatures exhibited in each case are listed in Table 6.

W_{wg} (μm)	Power (W)	Peak temperature (K)
15	20	167
10	20	185
5	20	217

Table 6 Combinations of W_{wg} and power and the resultant value of peak temperature calculated.

This simulated driving a narrow laser with high input current (high power) in an attempt to achieve higher optical output powers. It can be seen that such an attempt results in a large temperature elevation of the laser active region which will, in turn, reduce the laser efficiency so that it is likely that little gain in optical output power is achieved.
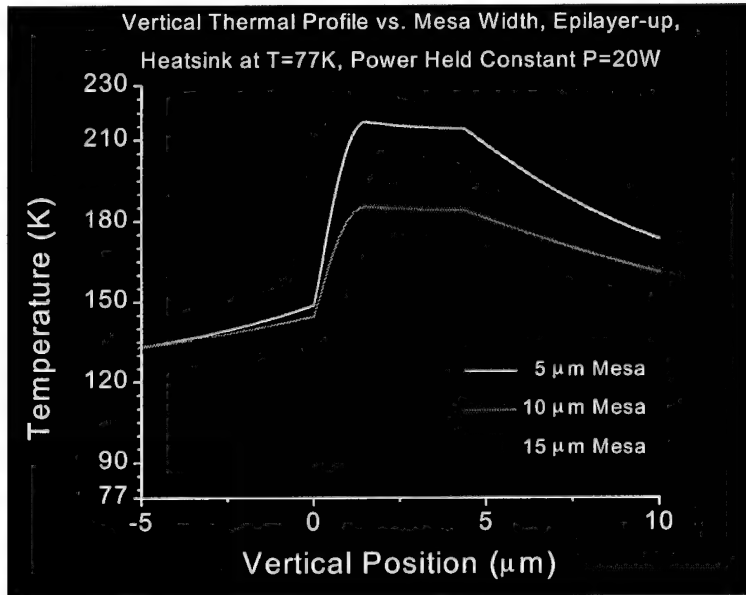
Figure 18 Calculation of the temperature profile through a vertical cross-section of the QCL with the heatsink temperature set to T = 77 K. The calculation is shown for different values of mesa width (in the lateral direction), keeping the input thermal power in the 'Active Region' constant in each case, P =20 W.
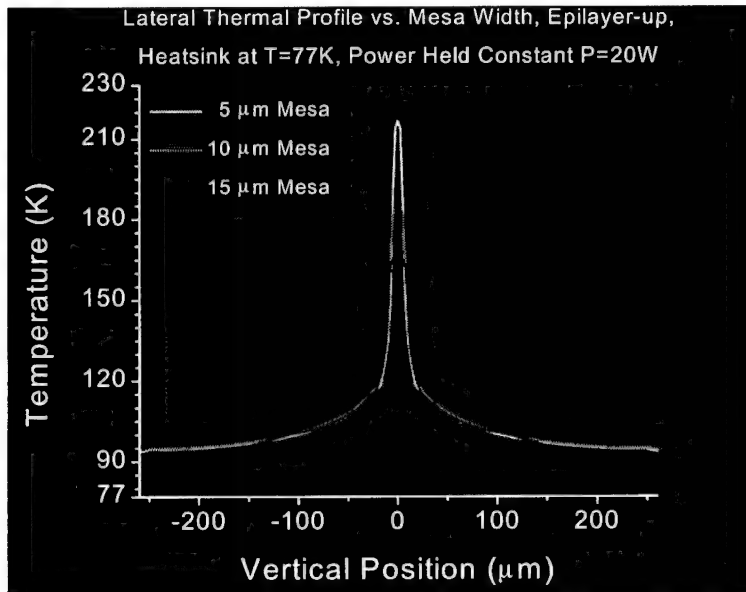

Figure 19 Calculation of the temperature profile through a lateral cross-section (along active region/upper cladding interface) of the QCL with the heatsink temperature set to T = 77 K. The calculation is shown for different values of mesa width, keeping the input thermal power in the 'Active Region' constant in each case, P =20 W.

Note that, although a combination of P = 6.66 W and W_{wg} = 15µm, would obviously give the lowest temperature rise, this combination might not be practical for a real laser, as the threshold current (power) required to achieve lasing scales with the laser width.

The conclusion which can be made from these two sets of calculations is that narrow mesa are key to achieving CW operation since they are capable of producing laser emission without incurring large temperature elevations in the active region. However, we require a much greater optical output power than attainable from a single narrow mesa. In order to obtain a high optical output power an array of narrow mesa should be investigated. Operating a number of narrow mesa in parallel may have the potential to increase the output power while retaining the benefits of the narrow mesa.

6.4 Simulation results for Array QC Lasers

Simulations were carried out for an array of three 5µm-wide (W_{wg} = 5µm) mesa, spaced D_{array} apart on a 500µm-wide chip (refer to Figure 14). Again, the temperature of the outer boundaries of the geometrical representation were set to T = 77 K to imitate a heatsink held at liquid nitrogen temperature. The total power of P = 20 W was divided equally between the three mesa in the array so that each mesa was 'supplied' with 6.66W of thermal power. The simulation was performed for a range of values of D_{array} which are listed in Table 7 along with the peak temperatures calculated for each member of the array. The values of temperature were taken from the lateral thermal profile across the chip (that is the temperature calculated along the lateral cross-section at the active region/upper cladding interface), shown in Figure 20. The profile of a single 15 µm-wide mesa being operated under the same conditions, is also displayed for comparison.

Mesa Spacing -	Peak Temperature - T (K)		
D_{array} (µm)	Left-hand Mesa	Centre Mesa	Right-hand Mesa
30	133.3	136.8	133.3
50	132.6	134.9	132.6
75	131.0	133.7	131.0
100	129.8	129.3	129.8
150	**127.5**	**129.1**	**127.5**
200	128.5	126.7	128.5

Table 7 Values of peak temperature calculated for a range of mesa spacing.
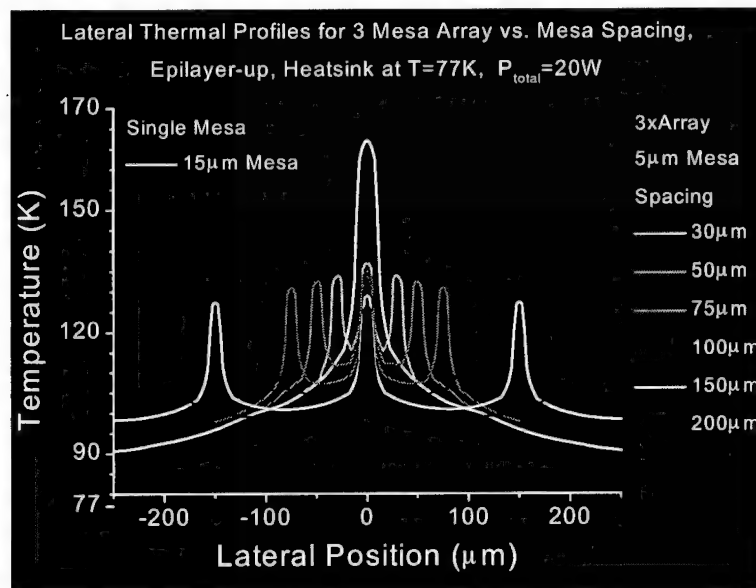

Figure 20 Graph of the lateral temperature profile calculated across the laser chip for a range of mesa spacing D_{array}.

The temperature elevations for all values of D_{array} tried were significantly lower than the equivalent single mesa obtained when the three components of the array merge into one (maximum peak temperature difference of ~40 K). The variation in the peak temperature between the arrays of different

D_{array} was lower, with a maximum difference in peak values of ~10 K. From the profiles in Figure 20, the trend as the D_{array} increases was that the heat generated was spread out such that the temperature rise was more uniform across the laser chip.

Doubling the spacing from 50 μm to 100 μm, decreased the temperature of the central mesa by 5.6 K, whereas doubling the spacing from 100 μm to 200 μm only resulted in a further decrease of just 2.6 K. Therefore, for a laser chip with a substrate thickness of $H_{sub} = 150$ μm, a spacing $D_{array} \sim 150$ μm would appear to be appropriate.

6.5   Simulation results for Array QC Lasers mounted Epilayer-down

An identical set of simulations were carried out on the geometrical layout depicted in Figure 22, which represents a QC laser mounted epilayer-down on a copper heatsink using indium bonding. Epilayer-down mounting is commonly employed to improve the performance of semiconductor lasers, and has recently been used to improve the performance of conventional QC lasers. [5]
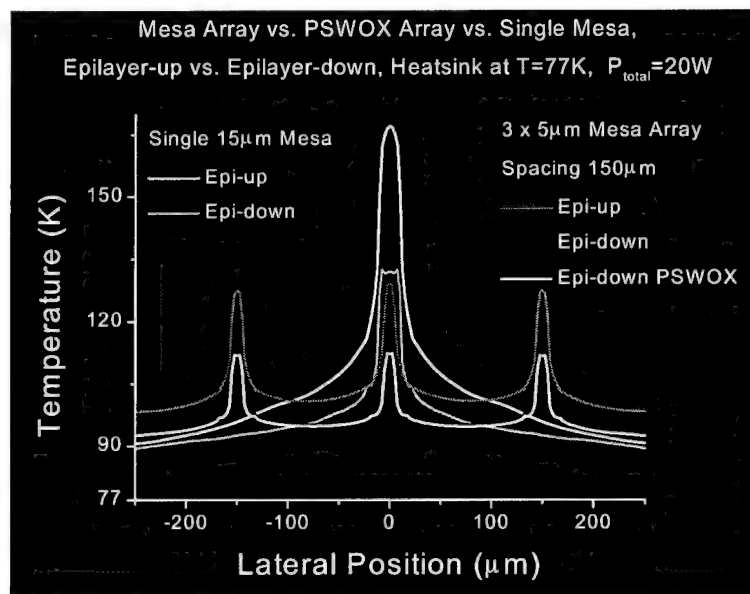

Figure 21. Calculation of the temperature profile through a lateral cross-section (along active region/upper cladding interface) of the various QCL designs mounted epilayer-up and epilayer-down. The heatsink temperature set to T = 77 K and the input thermal power in the 'Active Region' the same in each case, P =20 W.

A summary of the results obtained are shown in Figure 21. The figure shows the graph of the lateral temperature profile and includes simulation results obtained for the 3 x 5μm mesa array mounted epilayer-down, the 3 x 5μm mesa array mounted epilayer-up for comparison, a 3 x 5μm PSWOX mesa array (10 μm-wide, 2.5 μm deep alumina moats) mounted epilayer-down, a 15 μm-wide single mesa mounted epilayer-down, and a 15 μm-wide single mesa mounted epilayer-up for comparison.

The simulations indicate that further substantial improvements may be obtained if the lasers are mounted epi-layer down. According to these simulations, the best performance was obtained using the PSWOX QCL array mounted epilayer-down, although the improvement over the mesa-etched QCL array mounted epilayer-down was slight.

Care must be taken here, however, since the model neglects the effect of doping and the effect of the superlattice active region on the values of the thermal conductivity. These effects would be particularly noticeable when the devices are mounted epilayer-down, since the main flow of heat would be through the upper cladding layers which are, in fact, quite highly doped.
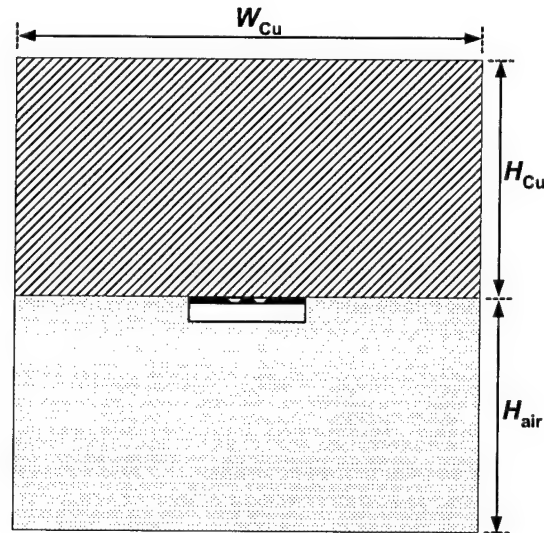
Figure 22. Geometric representation of the QC laser chip mounted epilayer-down onto a copper heatsink of width W_{Cu} and thickness H_{Cu}. The area, W_{Cu} by H_{air}, above the copper mount and laser chip is filled with 'air' (helium in our case).

A discrepancy between active region temperatures predicted by 1D non-linear finite element analysis and active region temperatures indicated by the performance of actual QCL devices mounted epilayer-down, was reported by Gmachl *et al.*[5] They believed that the difference was perhaps due to a combination of the simplifications made such as (3) and (5) listed previously in the assumptions/simplifications section of this document.

3. The active region was assigned a thermal conductivity of bulk ternary material. This simplification ignores the reflection of phonons (heat) at each InAlAs/InGaAs interface in the superlattice. In practice this phenomenon would make the effective thermal conductivity of the superlattice anisotropic. The value of K_y, the thermal conductivity perpendicular to the semiconductor layers, would be reduced with respect to K_x.

5. The values of thermal conductivities used were those reported for un-doped layers; values for doped semiconductors may be significantly lower. The modelling was performed on what was effectively an undoped semiconductor laser, whereas doping levels in a quantum cascade laser can be high and vary throughout the epilayer (see Table 4). Addition of doping atoms to the crystal lattice may create crystalline imperfections upon which phonons will scatter, decreasing the thermal conductivity. Towards room-temperature, the dependence of the thermal conductivity on doping level may be weak, since at high temperatures phonon-phonon scattering should dominante. At low temperature, where phonon-phonon scattering is weak, the phonon-impurity scattering will dominate, and the value of K will with drop with increasing doping levels. The values of temperature calculated by the modelling, should therefore be more accurate towards room-temperature. The temperatures calculated should always be an underestimate of the actual temperature since the thermal conductivity is over estimated at low temperatures.

If these simplifications are the culprits, then they should both decrease vertical heat extraction from the active region; lateral heat flow will become more important. In this case, the PSWOX QC laser should outperform the mesa-etched QC laser arrays, since they provide material adjacent to the mesa which may assist the lateral flow of heat.

The thermal modelling does justify our original design concept; under the same conditions of total power supplied to the chip a smaller peak temperature rise is anticipated for the arrays compared a

single stripe laser. However, other groups[7] have found that conventional finite element modelling of heat flow in Quantum cascade laser, although successfully predicting trends it has not been accurate in predicting thermal operating characteristics. One explanation is that this may be due to the layer structure of active region (there are up to 400 layers) may result in an anistropic heat conduction (the finite element model assumes isotropic heat conduction) and that probably heat conduction parallel to the layer is larger than heat conduction perpendicular to the layers. It is difficult to estimate the size of these effects and, at this stage, rather than speculate or make theoretical estimates, it would be more productive to measure the temperature distribution of an operating quantum cascade laser, perhaps using techniques such as microRaman[8].

7   Conclusions

In this report we have presented an investigation into laser bars of intersubband mid infrared semiconductor lasers based on quantum cascade laser arrays operating at wavelengths close to 5µm; we have covered the design, fabrication and characterisation of these laser arrays and have covered the thermal modelling of these laser arrays. As far as we are aware this is the first investigation into Quantum Cascade Laser arrays.

The temperature dependence of the threshold current as characterised by T_0 is around 136K which shows some improvement on single stripe lasers operating at similar powers. The mode profile from the laser array show three peaks which we expect from 3x1 array. For some applications such as IR laser illumination these mode profiles are acceptable. The light-current results show that the 3x1 laser arrays on the A1376 wafer have average powers of around 1-4mW when operated in pulsed mode with input average electrical powers in the range 50mW-200mW . In summary the QCL arrays have been demonstrated, the mode profiles are reasonable for some applications. The T_0 are improved, providing some evidence of the advantage in thermal arrays in reducing peak temperatures, confirming by the predictions made by thermal modelling. However, the powers are low, but the wafer we have employed, A1376, appears not to be as efficient as the same wafer design reported in reference 4.

Our results indicate, by simple scaling, that to obtain 250 mW average power per facet at temperatures greater than 77K, from the laser array approach would require an array of 190 stripes and a heat sink capable of extracting 12.5W. This number of stripes would require unrealistically large amounts of wafer and therefore the array laser approach 250mW average power operation at temperature >77K seems limited.

From our investigation we can make the following recommendations:

- A more efficient quantum cascade laser wafer design is required.
- Epitaxial side heat sinking would be helpful.
- To complement the thermal modelling, the thermal distribution in an operating QCL array is experimentally investigated by a technique such as microRaman.
- New fabrication techniques are investigated such as PSWOX (see Appendix 1).
- Longer QCL laser arrays greater than 2.6mm employed here.

[7] "Improved CW operation of Quantum Cascade Lasers with Epitaxial side Heat Sinking" C. Gmachl, A. M. Sergent, A. Tredicucci, F. Capasso, A. L. Hutchinson, D. L. Sicon, J. N. Baillargeon, S. N. G. Chu and A. Y. Cho, IEEE Photonics Tech. Letts. 11 1369 1999
[8] see for example "Raman microprobe study of the time development of AlGaAs single quantum well laser facet temperature on route to catastrophic breakdown" W. C. Tang, H. J. Rosen, P. Vettiger and D. J. Webb, Appl. Phys. Letts. 58 557-559 1991.

APPENDIX 1

PSWOX Technique

Appendix 1 contains a recent manuscript sent to Applied Physics Letters for consideration of publication. The work is, as yet, unpublished and should be considered confidential.

A quantum cascade laser fabricated using planar native-oxide layers

C. D. Farmer[a]
Department of Electronics & Electrical Engineering, University of Glasgow, Glasgow G12 8LT, UK.

P. T. Keightley
Department of Physics and Astronomy, University of Sheffield, Sheffield S3 7RH, UK.

C. N. Ironside and C. R. Stanley
Department of Electronics & Electrical Engineering, University of Glasgow, Glasgow G12 8LT, UK.

L. R. Wilson and J. W. Cockburn
Department of Physics and Astronomy, University of Sheffield, Sheffield S3 7RH, UK.

Abstract: We present the first work on the application of a thermal wet oxidation process to the fabrication of quantum cascade lasers. The native oxide of the Al0.48In0.52As upper cladding layer was formed and used to provide electrical and optical confinement for lasers operating at $\lambda \approx 5$ μm. Initial results include 1.4 W peak output power and 0.69 W/A slope efficiency at 10 K, and a reduced temperature dependence of the threshold current density (T0 = 142 K).

Since the invention of the quantum cascade (QC) laser in 1994 by Faist et al.,[1] these mid-infrared emitters have undergone rapid development. QC lasing has been demonstrated in both the InP-$In_{0.53}Ga_{0.47}As$-$Al_{0.48}In_{0.52}As$ and GaAs-$Al_xGa_{1-x}As$ materials systems.[2] The native oxides of III-V semiconductors formed by thermal wet oxidation have become important materials for many optoelectronic devices since their development began a decade ago.[3,4] The oxides formed by this reaction are stable, have a low refractive index and good electrical insulation making them extremely useful in semiconductor laser fabrication (for a review see, for example Ref. 4). The process was first demonstrated by Holonyak and his co-workers in the GaAs-$Al_xGa_{1-x}As$ system,[3] and later extended to materials lattice-matched to InP by Caracci et al.[5], where the native oxide of $Al_{0.48}In_{0.52}As$ was employed in gain-guided conventional lasers. In planar (vertical) selective thermal wet oxidation (PSWOX) the reaction begins at the AlInAs surface and proceeds downwards through the semiconductor epilayer, using H_2O to convert the AlInAs into an oxide which is mainly composed of an amorphous matrix (AlO_x, As), with inclusions of crystallised In_2O_3.[6] We present the first work on the application of a PSWOX process to the fabrication of InP-$In_{0.53}Ga_{0.47}As$-$Al_{0.48}In_{0.52}As$ quantum cascade lasers.

QC lasers usually employ an etched mesa structure for electrical and optical confinement, but the removal of material adjacent to the mesa means that there is a reduction in the lateral heat extraction. Heat dissipation is of prime importance in QC lasers, owing to the high electrical power required for operation and the dependence of performance on the non-equilibrium phonon population.[7] We report a fabrication technique applied to a QC laser design which provides electrical and optical confinement by conversion (rather than removal) of the $Al_{0.48}In_{0.52}As$ upper cladding to a native oxide. The initial results are presented which show that the technique produces QC lasers with high output power, high slope efficiency and a reduced temperature dependence of the threshold current (larger T_0) compared to their mesa-etched counterparts.

The layer structure was grown by solid source molecular beam epitaxy (MBE) using As_2. It used an AlInAs ternary upper cladding layer and was based on a design first reported by Faist et al..[1] We used a 20 nm-thick InGaAs contact layer doped with Si to $N_d \approx 2 \times 10^{19}$ cm^{-3}. Processing commenced with the

---

[a] Electronic mail: c.farmer@elec.gla.ac.uk

deposition of a 200 nm layer of silica by plasma-enhanced chemical vapour deposition (PECVD). Two 60 μm-wide windows, separated by 20 μm, were made through the silica using photolithography and wet etching. Removal of the 20 nm InGaAs contact layer and underlying 28 nm graded superlattice region was carried out by wet etching in a 1:1:200 H_2SO_4:H_2O_2:H_2O solution. This exposed the 2.5 μm-thick AlInAs upper cladding layer, ready for the subsequent thermal wet oxidation. The remaining silica mask formed a barrier to the water vapour during the wet oxidation and only the uncovered areas were converted to the native oxide. The sample was placed in a nitrogen-purged reaction furnace at 500 °C which was then supplied with 0.5 litre/min of nitrogen bubbled through a flask containing de-ionised water held at 98 °C for a duration of 90 minutes. Using photolithography and dry etching with a C_2F_6 plasma, an 8 μm-wide contact window was made in the 20 μm-wide silica stripe between the two wet oxidised regions. The existing silica oxidation mask was left elsewhere to serve as the electrical insulation layer. A Ti/Pd/Au layer was evaporated as a contact to the epi-layer and an Au/Ge/Au/Ni/Au layer was deposited on the substrate after thinning to ~170 μm. The sample was cleaved into 2 mm (±0.1 mm) long laser bars and soldered epi-layer up onto a TO-5 header with indium solder. Gold-wire connections were made to the Ti/Pd/Au contact using ultrasonic bonding.

From a fabrication-based point of view this method of producing QC lasers has a number of advantages. The planar design facilitates epi-layer down mounting, and simplifies the alignment of the contact window. In fact, the alignment of a contact window can be completely avoided if the entire surface area between adjacent laser waveguides is permitted to oxidise. A subsequent dry etch with C_2F_6 removes the silica oxidation mask, but leaves the native oxide intact, allowing a self-aligned process, and thereby reducing the total number of photolithographical steps required for Fabry-Perot QC lasers to just one.

Fig. 1(a) shows a scanning electron microscope (SEM) cross-section of the completed PSWOX QC laser at the edge of the oxidation mask. The SEM shows a darkened region extending ~ 0.65 μm down from the upper surface of the AlInAs cladding. Here the semiconductor has been exposed to the steam and is labelled 'native oxide'. Below the AlInAs upper cladding lies the QC laser waveguide core. The core contains nearly 500 lattice matched AlInAs and GaInAs layers sandwiched between two 300 nm GaInAs layers. Fig. 1(b) shows a plan view image of a section of the laser before the final metallisation has been carried out. In the centre, running vertically, is the 20 μm-wide optical waveguide. The lighter bar in the centre of the waveguide corresponds to the region where the silica oxidation mask has been removed to form the 8 μm-wide contact window. The 60 μm-wide dark regions on either side of the waveguide are the native oxide layers. The subsequent metallisation step makes contact to the waveguide through the 8 μm-wide contact window and, the lateral spread of injected current is limited by the non-conducting oxide regions. Furthermore, the low refractive index of the oxide (n ≈1.67 at λ=1.55 μm)[6] provides optical confinement in the lateral direction. The limited depth of this oxide region implies that these lasers are equivalent to rib mesa QC lasers (see, for example, Ref. 8).

For characterisation, the lasers on the TO-5 header were mounted on the temperature-controlled cold-head of a closed-cycle helium-flow cryostat and driven with 50 ns current pulses with a repetition rate of 1kHz. Emission from the laser was collected and focused via two gold-coated parabolic mirrors into a Bruker IFS55 Fourier transform infra-red (FTIR) spectrometer operating in step-scan mode with a resolution of 0.5 cm^{-1}. Fig. 2 shows the spectrum of the light from a 2mm long PSWOX QC laser taken at 10K with a drive current of 3.70 A. The longitudinal Fabry-Perot mode structure is clearly visible and the measured mode spacing of ~ 0.75 cm^{-1} indicates a modal effective index of n_{eff} = 3.3 ± 0.2, agreeing with the value of n_{eff} =3.27 calculated for the fundamental mode of the waveguide.

Fig. 3 shows the light-current curves for the same device at different heat sink temperatures. The laser emission was measured with a calibrated, liquid nitrogen-cooled Graseby mercury cadmium telluride (MCT) detector. Output power levels and temperatures requiring drive currents greater than 4.5 A were not investigated because of the limitations of the current pulse generator used. For the power measurements reported below we have assumed a collection efficiency of 100% per facet and the power measurements will therefore tend to be an under estimate of the actual output power level. At 10 K, the PSWOX device has a threshold current of I_{th} = 2.4 A. An optical output power of 1.4 W was measured from a single facet at a drive current of 4.5 A. A best fit of the data at 10K shows a very high average slope efficiency of 0.69 W/A for a single facet. Calculating the slope of the graph of heatsink temperature versus ln(I_{th}) yields a characteristic temperature of T_0 = 129 K, where I_{th}∝exp(T/T_0). We have also measured T_0 values of 138 K and 142 K for two other PSWOX lasers of identical dimensions, fabricated on the same 6 mm by 5 mm portion of wafer, but mounted epi-layer-up on a copper block (rather than a TO-5 header). These values compare with a T_0 value of 110 K for a laser fabricated from the same wafer but using a conventional mesa fabrication method, and with a T_0 value of 114 K report by Faist et al.[1] with a similar wafer design and mesa-etched laser. We attribute the

improved T_0 of the PSWOX QC lasers to a reduction in the thermal resistance through enhanced lateral heat extraction. Similar improvements in the value of T_0 have been reported for rib-mesa or "shallow-etched" mesa in QC lasers in which only the upper cladding was removed.[8] A direct comparison of T_0 values is not possible since these QC lasers were based on different QC wafer designs emitting at other wavelengths.

Additional evidence indicating that optical confinement is provided by the native oxide can be deduced from the far-field emission patterns of the laser. Figure 4 compares the far-field scan taken normal to the epitaxial layers (vertical profile) with that taken parallel to the layers (horizontal or lateral profile). In both measurements the laser was operated in pulsed mode at 10 K. The MCT detector (1 mm x 1 mm element size) was scanned across the output beam at a distance of ~ 40 mm from the laser facet. In the vertical direction, the optical mode is strongly confined by the thin epitaxial layer. Calculation indicates that the majority of the fundamental mode is confined within ~ 3μm of epitaxial material due to the plasma-enhanced optical confinement.[1] As expected, the measured vertical profile was broad, concurrent with emission from an aperture comparable in dimension to the wavelength of the emitted light. The measured horizontal profile, in which the optical mode was confined by the native oxide, was ~ 6 times narrower than the vertical profile indicating, from first order diffraction theory, that laser emission in the lateral direction originated from an aperture of ~ 18μm in width. This accords with the measured aperture width of ~ 19 μm obtained from SEM measurements.

In conclusion, we have reported a new method for fabricating quantum cascade lasers which uses native oxide to define a current aperture and waveguide. Like rib-mesa structures, this fabrication technique has produced QC lasers which have improved performance, including reduced temperature dependence of the threshold current along with high output powers. We are currently investigating the use of higher drive currents which are required for higher temperature and output power operation, deeper oxide layers for improved current confinement, and studies of the thermal and mid-infrared optical properties of the native oxide of $Al_{0.52}In_{0.48}As$.

List of References

[1] J. Faist, F. Capasso, C. Sirtori, D.L. Sivco, J.N. Baillargeon, A.L. Hutchinson, S.G. Chu, A.Y.Cho, Appl. Phys. Lett. 68, 3680 (1996).

[2] C. Sirtori, P. Kruck, S. Barbieri, P. Collot, J. Nagle, M. Beck, J. Faist, U. Oesterle, Appl. Phys. Lett. 73, 3486 (1998).

[3] J. M. Dallesasse, N. Holonyak, Jr., A. R. Sugg, T. A. Richard, and N. El-Zein, Appl. Phys. Lett. 57, 2844 (1990).

[4] R. D. Dupuis, Compound Semicond. 3, 32 (1997).

[5] S. J. Caracci, M. R. Krames and N. Holonyak, Jr., J. Appl. Phys. 75, 2706 (1994).

[6] P. Petit, P. Legay, G. Le Roux, G. Patriarche, G. Post and M. Quillec, J. Electron. Mat. 26, L32 (1997).

[7] M. Razeghi, Microelectron. J. 30, 1019 (1999).

[8] C. Gmachl, F. Capasso, J. Faist, A.L. Hutchinson, A. Tredicucci, D.L. Sivco, J.N. Baillargeon, S.G. Chu, A.Y. Cho, Appl. Phys. Lett. 72, 1430 (1998).

List of Figure Captions

FIG. 1. (a) SEM photo of the crossection of the PSWOX QC laser after metallisation and (b) a plan view photograph of the same waveguide before metallisation using an optical microsope.

FIG. 2. Emission spectrum at 10 K showing the longitudinal modes.

FIG. 3. Peak optical power versus drive current of the PSWOX QC laser at different heatsink temperatures;-•- linear fit of slope at 10 K. The inset shows a plot of I_{th} (log scale) versus temperature.

UNIVERSITY OF
GLASGOW
Optoelectronics
Research Group

FIG. 4. Normalised cross sections of the far-field emission patterns measured in the directions normal to the epitaxial layers (–•– vertical profile) and parallel to the layers (–♦– horizontal profile).
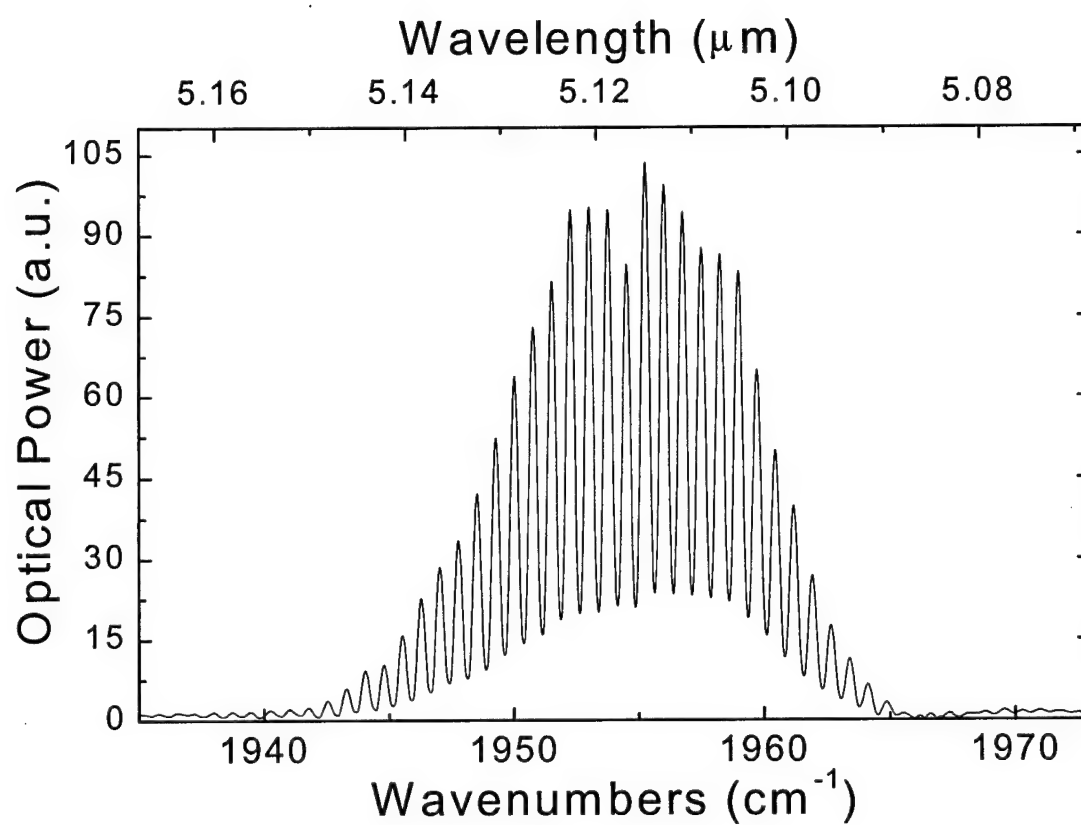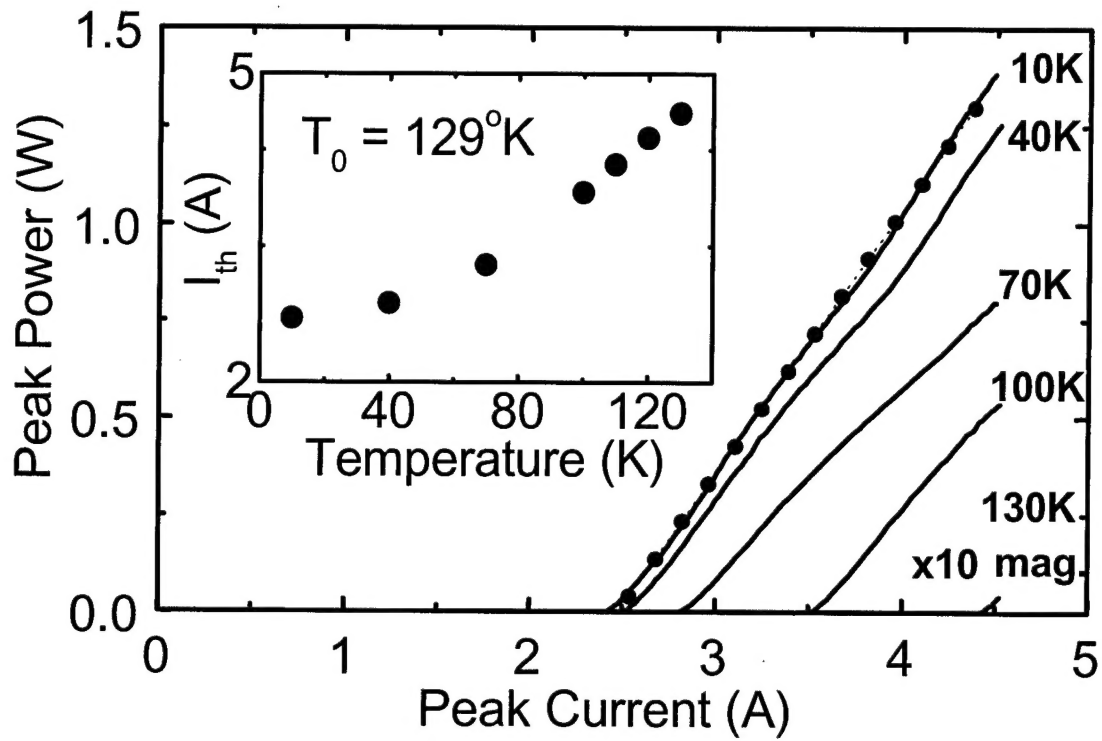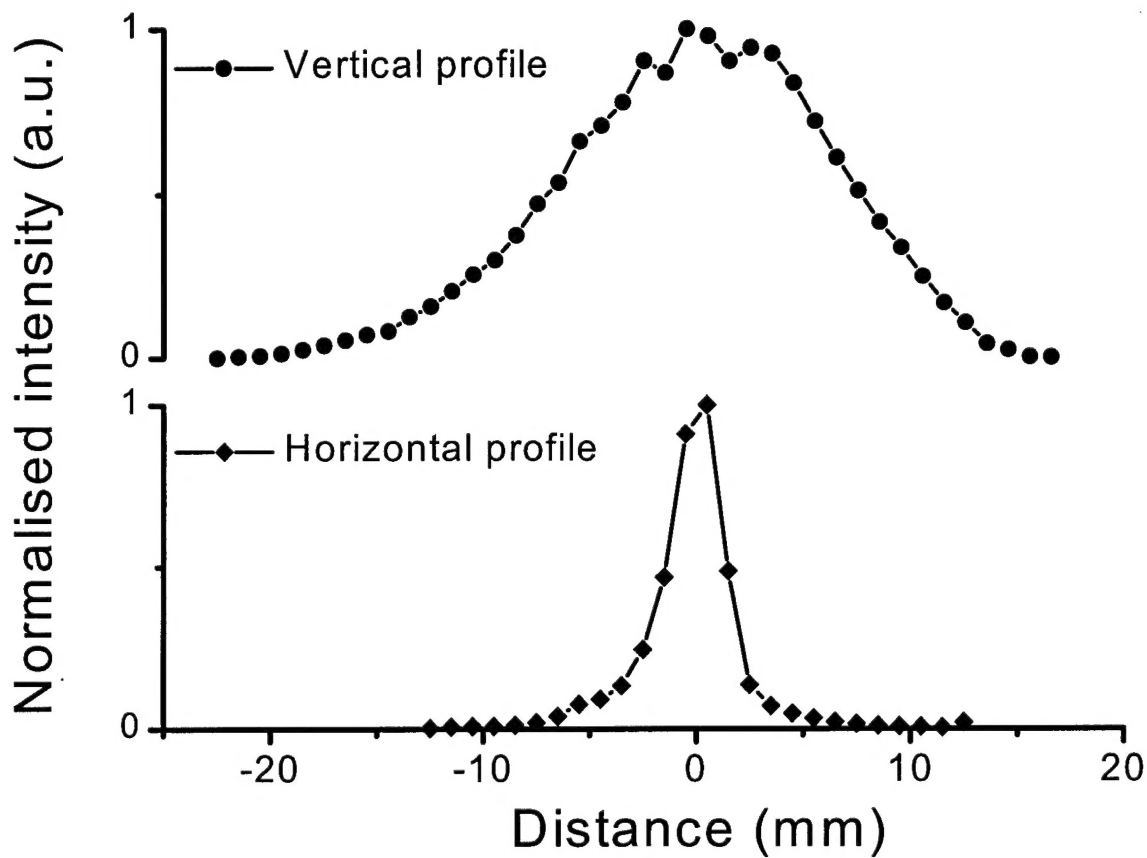
Figure 1, C. Farmer
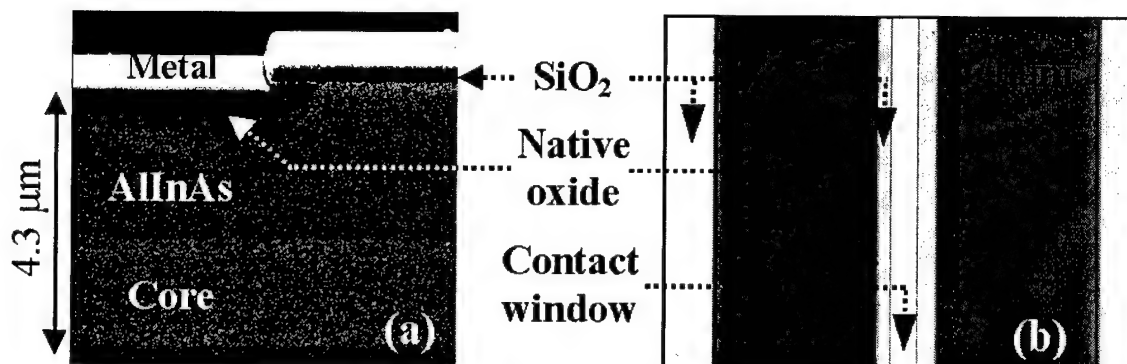
Figure 2, C. Farmer

Figure 3, C. Farmer

Figure 4, C. Farmer

Appendix 2

The ten laser chips supplied

There are ten laser chips supplied as part of the contact. They are in a gel container box for safe transport. The laser chips are made from wafer A1376. They are 3x1 arrays chips as described in the report.

Appendix 3

The mounted laser chip supplied

Although not in the original contract we have supplied a laser chip mounted on a copper heat, epilayer up. The copper heat sink is designed to fit in the CCC 1204 cryostat.